Results in Engineering 27 (2025) 106538

Contents lists available at ScienceDirect

Results in Engineering

journal homepage: www.sciencedirect.com/journal/results-in-engineering

Research paper

Impact absorbing pavement provides head protection comparable to helmets in oblique impacts

Christina Makoundou [a,c,1,2], Qi Huang [b,*,1], Chengbin Li [b], Zhou Zhou [b], Svein Kleiven [b], Cesare Sangiorgi [c]

[a] Sustainable Pavements and Asphalt Research (SuPAR), Faculty of Applied Engineering, University of Antwerp, 2020 Antwerp, Belgium
[b] Division of Neuronic Engineering, KTH Royal Institute of Technology, Stockholm, 14157, Sweden
[c] Department of Civil, Chemical, Environmental and Materials Engineering, University of Bologna, Bologna, 40131, Italy

ARTICLE INFO

Keywords:
Impact-absorbing pavement
Oblique impacts
Head injury metrics
Finite element analysis
Vulnerable road user

ABSTRACT

Head injuries constitute an increasing public health concern. Although motor vehicle injuries have steadily declined in Sweden, the number of injuries and fatalities among unprotected vulnerable road users (VRUs) continues to rise. Inspired by playground surfaces, rubberized asphalts have recently been developed as impact-absorbing pavement (IAP), with the dual objectives of enhancing collective safety and minimizing injuries, while promoting higher-value applications within the waste hierarchy. This study aims to biomechanically evaluate IAP's head injury protection performance by conducting laboratory oblique impact tests to obtain impact kinematics and finite element (FE) simulations to estimate brain strain responses. A total of 30 impact tests were performed on five kinds of asphalt samples under three impact locations. Eleven kinematics-based and five strain-based head injury metrics were analyzed and compared. For example, the peak linear acceleration (PLA), peak angular velocity (PAV), and max principal strain (MPS) were lower than 150 g, 36 rad/s, and 0.4 during oblique impact against the IAP prototype. The results demonstrated that the IAP achieved a comparable head protection performance to helmets, indicated by both the linear-based and rotational-based head injury metrics at 6 m/s. These findings show that IAP has significant potential to reduce head injuries among unprotected VRUs and contribute to a safer traffic environment.

1. Introduction

Traumatic brain injury (TBI) constitutes an increasing public health concern worldwide. Although motor vehicle injuries have steadily declined in Sweden, the number of injuries and fatalities among vulnerable road users (VRUs) continues to rise [1]. VRUs primarily include pedestrians and bicyclists, who are at a greater risk of sustaining severe injuries in traffic crashes, and thus require enhanced protective countermeasures. According to the National Highway Traffic Safety Administration (NHTSA, 2021) [2], the proportion of traffic fatalities among VRUs increased from 28% in 1980 to 34% in 2019. Furthermore, reports from the Federal Highway Administration (FHWA) indicate the percentage of VRUs fatalities from 2011 to 2020 was higher than that of total traffic fatalities [3]. Injury data from Swedish cyclists also demonstrate that head injuries are more likely to result in permanent medical impairment compared to other trauma types [4]. With the increased use of alternative modes of transportation [5], the urgency to address TBI among VRUs is expected to rise further, necessitating effective prevention strategies [6].

Currently, most road surfaces are constructed from stiff asphalt, composed of crushed stone bound by bitumen, which provides little protection and leaves the VRUs (e.g., cyclists) reliant primarily on personal protection equipment (e.g., helmet) [7]. Inspired by playground surfaces, impact-absorbing pavement (IAP) is being developed in which a portion of the crushed stone is replaced with rubber granules derived from recycled car tires [8]. The IAP concept was developed as the starting point for a design regeneration-rethinking approach for safer roads and implementing green policies to encourage people to cycle or walk

* Corresponding author at: Hälsovägen 11C, 141 57 Huddinge, Sweden.
E-mail address: qihuang@kth.se (Q. Huang).
[1] These authors contributed equally to this work as co-first authors.
[2] Present address: University of Antwerp, Sustainable Pavements and Asphalt Research (SuPAR), Department of Construction Engineering, Antwerp, 2020, Belgium.

https://doi.org/10.1016/j.rineng.2025.106538
Received 10 June 2025; Received in revised form 25 July 2025; Accepted 30 July 2025

Available online 6 August 2025

instead of massively using cars. The role of such material is to make the sidewalks and/or bike lanes surface layer less dangerous and reduce possible human injuries resulting mainly from falls [9]. This promising approach aims to enhance the impact-absorbing capability without altering the inherent properties of pavement [10].

The IAP materials differ from conventional rubber-modified asphalts in that they incorporate a significantly higher proportion of crumb rubber derived from end-of-life tires [11]. They also differ from playground rubber tiles by including a lithic skeleton composed of mineral aggregates in their formulation [12]. This structural design enhances impact-absorbing performance while simultaneously improving the mechanical response and load-bearing capacity of the pavement [9]. The use of end-of-life materials in asphalt not only addresses environmental concerns and reduces economic costs [13–15], but also contributes to improving the safety of urban roadways. Additionally, sidewalks and pedestrian areas can benefit from IAP, which provides passive protection for collective safety, independent of individual protective devices. Rubber playground materials have been successfully used for years as paving materials to minimize injuries in children's parks or similar [16], while the possibility of adapting IAP to roads - that would mean that the material should be able to reduce the risks of injuries for VRUs in urban areas and be possibly produced, laid, and maintained using already known road paving methods- has started to be developed into roads and explored recently in terms of use in real case scenario and case of potential fall on it [17,18].

However, there is a lack of methods to evaluate the head protection performance of IAP biomechanically. Preliminary studies [19,20] employed a hemispherical aluminum impactor (according to EN 1177 : 2018+AC:2019 standard, the Head Injury Criterion Meter) to measure the linear acceleration attenuation of the flat surface during a free fall. Nevertheless, the direct vertical impact conditions with primary linear motion neglect the aspects that oblique impacts (with both linear and angular motions) are more common in real life, and the angular-related motion is the primary cause of brain trauma. Real-world cyclist head impacts are more complex than the current test standard. They typically occur as oblique impacts, involving both normal and tangential incident velocities that generate a combination of linear and rotational kinematics [21,22]. Linear kinematics are associated with pressure gradients that can cause focal injuries such as skull fractures [23], whereas rotational kinematics are highly correlated with brain tissue shear strain, leading to injuries like concussions or diffuse axonal injuries [24,25]. Therefore a 45° oblique impact emerges as a more suitable and reliable approach for head protection assessment of IAP since this angle falls central to a range of reported cyclist head impact angles from simulation studies [26]. Oblique tests, including impacts by guided free-fall onto an angled anvil [27,28], frequently employ a Hybrid III (HIII) 50th percentile male anthropomorphic head and neck combination [29,30]. These kinematic measures are further used to define the loading of finite element (FE) models of the human head to study brain injuries [31,32].

In addition to experimental approaches, state-of-the-art computational methods are also widely used to investigate the injury protection of safety gears (e.g., helmets). Over the past decades, a variety of human head models with different levels of anatomical detail and modeling complexity have been incorporated to support brain injury research. One major advantage of FE head models is their ability to provide detailed predictions of the brain tissue response while preserving the anthropometric characteristics of the human head [12]. Moreover, continued efforts on integrating advanced machine learning techniques to predict injuries have also led to higher efficient tools [33–36].

The current study aimed to address how the IAP can improve head safety for unprotected VRUs in real traffic scenarios. To this end, we conducted oblique impact tests for different rubberized asphalts at three impact locations. The extracted experimental kinematics were then integrated into a biofidelic FE head model to predict the strain distribution and peak values. The head protection performance was evaluated based on both kinematics-based and strain-based injury metrics. This study provides new insights into the biomechanical evaluation of road safety solutions.

2. Materials and methods

2.1. Rubberized asphalt material

The materials developed, which contain 56% rubber by volume, were evaluated following up on field trials conducted in Imola, Italy, as detailed in a previous study [17]. Note that this study is intended for materials designed exclusively for use on pedestrian paths and bike lanes within urban settings. The material developed is significantly softer than traditional pavements and is specifically designed to function as an IAP, as it contains an unusually high rubber content - over 50% of the total mixture volume - compared to other rubberized asphalt pavements. The use of rubber is motivated by the objective of obtaining an elastic material that fosters the circular economy of tires in the transportation ecosystem.

This mixture was created by partially replacing a portion of the mineral aggregates (0 - 4 mm) with an equal volume and similar particle size distribution of rubber, using a Hot-Rolled Asphalt (HRA) sieving curve as a reference. The HRA is recognized for its relatively high content of fine aggregates compared to other standard mixes, which can enhance the structural matrix of the produced specimens. The final specimens contain 22% vol of aggregates and filler, and 56% vol of rubber (smaller than 4 mm). All the samples were produced at room temperature using the dry process coupled to a bitumen-based emulsion modified with SBS polymers (PmE) with a dosage of 21% by total mixture mass. Finally, 1% wt. of cement was used as an additive to the mixture and a breaking facilitator for the emulsion, the IAP components were illustrated in Fig. 1a). The mixing process lasted 1 to 2 minutes to have a fully coated and homogeneous mixture. This assessment was made using the organometallic procedure described in EN 12697-55. More information on the material properties could be projected from prior research [10] using the Uniaxial Compression Test. Both Uniaxial unconfined stress-relaxation test and the axial unconfined destructive compression procedure were performed in this study. The materials produced with the same quantity of rubber and cold procedure are much softer than materials containing less rubber and hot-mix procedure.

The mixtures were compacted using the gyratory compactor methods (EN 12697-31) to produce samples of 100 mm of diameter and 46 ± 1 mm thickness (see Fig. 1b). Multiple samples were produced for a various number of gyratory cycles namely 10, 20, 30 and 80 to compare the laboratory compaction to the field one [18]; nevertheless, to align with preliminary results, samples with the levels of compactions providing similar results with comparison to the on-site parameters, E30 and E80 (30 and 80 cycles) are the only considered for this study. The samples with the same formulation were artificially aged in the laboratory to produce EA30 and EA80 samples.

2.2. Oblique impacts setup

The oblique impact tests were conducted at the helmet lab at KTH Royal Institute of Technology. The oblique test contains an aluminum column, a non-moving concrete base, an angled anvil, and a HIII headform. A cantilevered arm held the headform in place during the free-fall and was automatically retracted before impact. The headform was inverted and placed on a U-shaped free-falling trolley that fell past a 45° anvil [37]. The 45-degree anvil setup has been widely adopted in oblique head impacts in recent studies [38–40] and is included as a standardized condition, such as the UN ECE 22.06. The rubberized asphalt samples were placed on the angled anvil and fixed by a C-shape structure to constrain the boundary during oblique impacts (see Fig. 1c).

The bare headform was then dropped onto the IAP directly at three impact locations (Fig. 2, referred to as Xrot, Yrot, and Zrot). Each impact was repeated two times at the same location using the same sample.

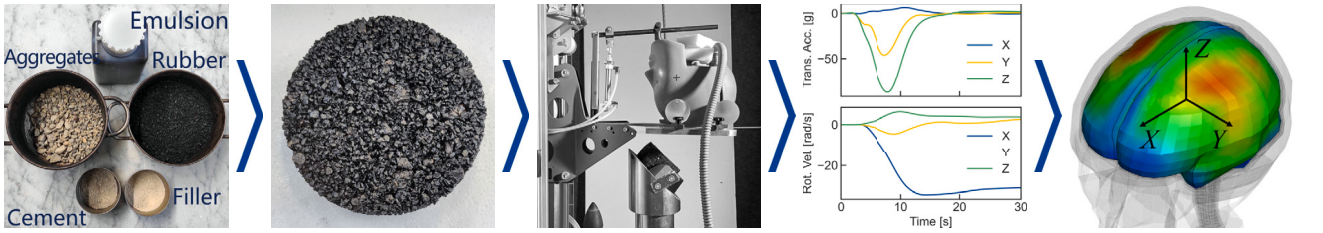

Fig. 1. Illustration of study design and methodology. (a) The rubberized asphalt used for impact-absorbing pavement (IAP) was composed of aggregates, emulsion, rubber granules, cement, and filler. (b) After cycling, the IAP sample was fixed to the angled anvil and integrated into the head drop test setup. (c) Oblique impacts were conducted using the HIII headform. (d) The three directions' kinematics, including linear acceleration and angular velocity, were recorded through the accelerometer inside the headform. (e) The experimental kinematics were imposed on the finite element head model to analyze the brain response.

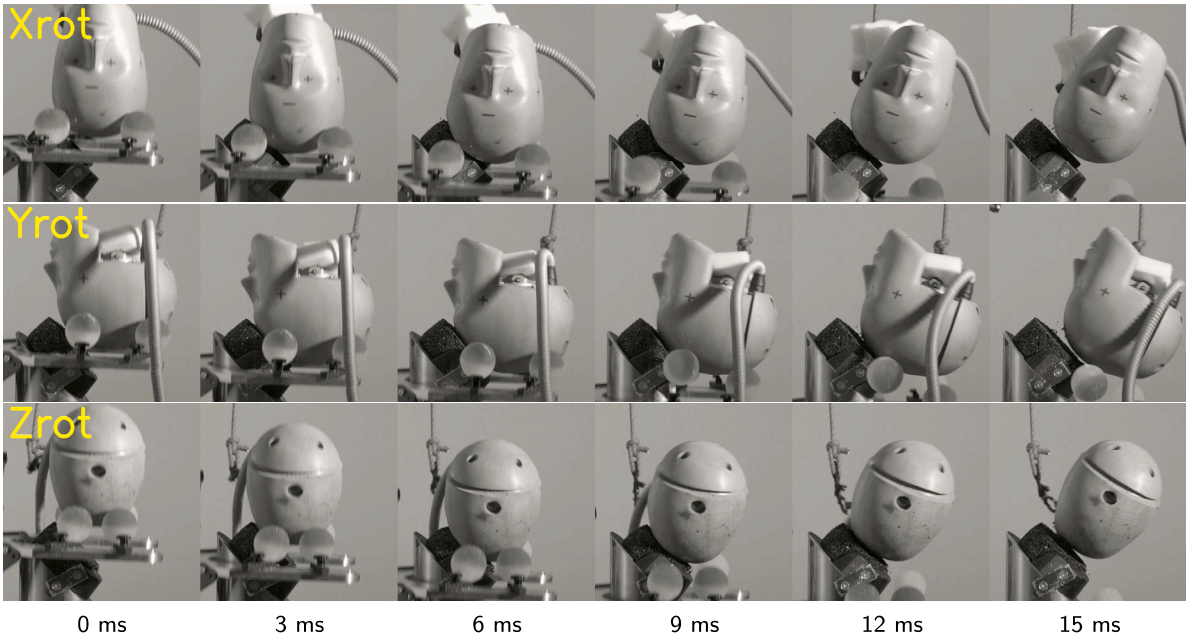

Fig. 2. Snapshots from the high-speed camera of the HIII headform oblique impacts against IAP E30 at three locations (Xrot, Yrot, and Zrot) from a drop height of 150 cm. Each oblique impact was recorded for 30 ms. Related kinematics were illustrated in the Appendix.

Four IAP samples, i.e., E30, E80, EA30, and EA80, were tested at a drop height of 150 cm, and another E30 was tested at 205 cm (which refers to E30_2, to achieve an impact velocity of 6.0 m/s). The drop height (150 cm) was according to the existing velocity adopted by the EN1078 standard for radial testing [41] to homologate bicycle helmets, and the impact angle (45°) corresponded to CEN TC158 (EU) New rotational test method [42]. In total, five IAP samples were tested in 30 oblique tests.

Six-degree-of-freedom headform kinematics were captured with a 3-2-2-2 accelerometer array sampled at 25 kHz [43]. All data channels were filtered with an SAE 180 filter with a cut-off frequency of 1000 Hz. The high-speed video was shot at 1000 FPS and checked after each test to make sure each test was performed as intended [7]. An example of head kinematics extracted from the headform was shown in Fig. 1d, which illustrated an oblique impact on the Xrot against IAP E30 from a 150 cm drop height.

2.3. Finite element simulations

To estimate the dynamic response inside the brain during the oblique impact, the experimental kinematics from the laboratory tests were applied to the FE head model (see Fig. 1e). The model was developed at the KTH Royal Institute of Technology by Kleiven [49]. It includes the scalp, skull, brain, meninges (i.e., dura mater and pia mater), intracranial membranes, cerebrospinal fluid, eleven pairs of the largest parasagittal bridging veins, and a simplified neck with the extension of the spinal cord. The brain was modeled as a homogeneous and isotropic structure, with its stress-strain nonlinearity represented by a second-order Ogden-based hyperelastic constitutive model and viscoelasticity by a six-term Prony series [49]. Detailed information regarding the geometric discretization, material properties of each head component, and the interface conditions between intracranial structures of the KTH head model can also be found in previous studies [53,54]. Responses of this model have shown a good correlation with experiments such as brain-skull relative motion [55] and intracranial pressure [56]. To enable the calculation of tract-related deformation of white matter, the axonal fiber tract was embedded within white matter [52]. Note that the fiber tract was only used in the post-processing procedure for strain calculation and did not have any mechanical contribution.

Fifteen FE simulations were performed according to five samples at three impact locations. The input kinematics for each simulation were derived from the mean values of two repeated tests, including directional linear accelerations and angular velocities, as shown in Fig. A.1. These six kinematic impulses were extracted from the accelerometer array embedded in the HIII headform and were applied to the center of gravity of the head model and constrained to the rigid skull [57]. All simulations lasted the same duration as the input kinematics (30 ms) and were conducted using an explicit dynamic solving method on a high-

Table 1
Eleven kinematic-based and five strain-based head injury metrics used in this study. Note that the coordinate system (XYZ) used to compute the kinematic-based metrics is the same as the laboratory tests.

Kinematics-based	Description	Notes
PLA	$\max(a(t))$	$a(t)$ is the resultant linear acceleration.
PAV	$\max(\omega(t))$	$\omega(t)$ is the resultant angular velocity.
PAA	$\max(\alpha(t))$	$\alpha(t)$ is the resultant angular velocity.
HIC [44]	$\max\left\{(t_2-t_1)\left(\frac{1}{t_2-t_1}\int_{t_1}^{t_2}a(t)dt\right)^{2.5}\right\}$	$a(t)$ is the resultant linear acceleration and t_2-t_1 is a time interval of 15 ms.
BrIC [45]	$\sqrt{\left(\frac{\omega_x}{\omega_{xc}}\right)^2+\left(\frac{\omega_y}{\omega_{yc}}\right)^2+\left(\frac{\omega_z}{\omega_{zc}}\right)^2}$	ω_x, ω_y, and ω_z are the maximal angular velocities along x-, y-, and z-axes, while ω_{xc}, ω_{yc}, and ω_{zc} are corresponding critical values (66.2, 59.1, and 44.2 rad/s) according to GHBMC brain model respectively.
UBrIC [46]	$\left\{\sum_i\left[\omega_i^*+\left(\alpha_i^*-\omega_i^*\right)e^{-\frac{\alpha_i^*}{\omega_i^*}}\right]^r\right\}^{\frac{1}{r}}$	$w_i^*=w_i/w_{icr}$ and $\alpha_i^*=\alpha_i/\alpha_{icr}$, where w_i and α_i $(i=x,y,z)$ are the maximum angular velocity and angular acceleration along x-, y-, and z-axes, w_{icr} are 211, 171, and 115 rad/s; α_{icr} are 20.0, 10.3, and 7.76 krad/s^2; r is 2, according to GHBMC brain model.
RIC [47]	$\max\left\{(t_2-t_1)\left(\frac{1}{t_2-t_1}\int_{t_1}^{t_2}\alpha(t)dt\right)^{2.5}\right\}$	$\alpha(t)$ is the resultant angular acceleration and t_2-t_1 is a time interval of 36 ms.
HIP [48]	$\max\left\{m\sum a_i(t)\int a_i(t)\mathrm{d}t+\sum I_{ii}\alpha_i(t)\int\alpha_i(t)\mathrm{d}t\right\}$	$m=4.5$ kg is the mass, I_{ii} is the principal moments of head inertia and i is the components of the acceleration in three axes according to a HIII dummy head.
KLC [49]	$k_1\max_t\lvert\omega(t)\rvert+k_2\ \mathrm{HIC}_{36}$	$k_1=0.004718$, $k_2=0.000224$ according to KTH head model, $\omega(t)$ is the maximum angular velocity, and HIC_{36} is HIC with a time interval of 36 ms.
GAMBIT [50]	$\max\left\{\left[\left(\frac{\lvert a(t)\rvert}{a_c}\right)^2+\left(\frac{\lvert\alpha(t)\rvert}{\alpha_c}\right)^2\right]^{1/2}\right\}$	$a_c=250$ g and $\alpha_c=25{,}000$ rad/s are the thresholds for the corresponding acceleration.
DAMAGE [51]	$\beta\max_t\{\lvert\vec{\delta}(t)\rvert\}$	β is a scalar factor set to 2.9903 according to GHBMC brain model; $\delta(t)$ is displacement time histories of the three coupled masses.
Strain-based	**Description**	
MPS	The maximum value of the 1st principal Green-Lagrange strain in the brain across the simulation.	
MTON [52]	The maximum value of normal strain oriented along the white matter fiber tract across the simulation.	
MTPN [52]	The maximum value of normal strain perpendicular to the white matter fiber tract across the simulation.	
MTOS [52]	The maximum value of shear strain oriented along the white matter fiber tract across the simulation.	
MTPS [52]	The maximum value of shear strain perpendicular to the white matter fiber tract across the simulation.	

performance computing system (HPE Cray EX supercomputer which features a CPU partition based on AMD EPYC processors, LS-DYNA revision 13.0.0, double precision) which details can be found in our previous studies [58–60].

Five strain-based metrics were employed (listed in Table 1) to evaluate how the rubberized asphalt influences the brain injury pattern. These included one brain tissue-level strain (maximum principal strain (MPS)) and four white matter tract-related strains (maximum tract-oriented normal strain (MTON), maximum tract-perpendicular normal strain (MTPN), maximum tract-oriented shear strain (MTOS), and maximum tract-perpendicular shear strain (MTPS) [61]). The MPS was extracted for all brain tissue elements ($N = 4{,}124$) and directly output from the simulation. These elements encompass major anatomical regions such as the cerebral cortex, brain stem, white matter, thalamus, cerebellum, and corpus callosum. In contrast, the tract-related strains were only computed for white matter elements ($N = 1{,}197$) with the exact mathematical equations in the previous study [62]. The peak strain values of all related elements were recorded during the oblique impact simulations.

2.4. Data analysis

Various brain injury criteria have been employed in TBI research, typically based on translational and/or rotational parameters of head kinematics, derived from experimental data fitting or reduced-order mechanical models [63,64]. In this study, we selected eleven kinematics-based head injury metrics (detailed in Table 1) to quantify head dynamic responses and IAP protection performance during oblique impacts. These metrics include two linear motion-based indices (peak linear acceleration (PLA) and head injury criterion (HIC) [44]), six rotational motion-based indices (peak angular acceleration (PAA), peak angular velocity (PAV) [38], Brain Injury Criterion (BrIC) [45], Universal Brain Injury Criterion (UBrIC) [46], Rotational Injury Criterion (RIC) [47], and Diffuse Axonal, Multi-Axis, General Evaluation (DAMAGE) [51]), and three metrics that combine both linear and angular motion (Head Impact Power (HIP) [48], Kleiven Linear Combination (KLC) [49], and the Generalized Acceleration Model for Brain Injury Threshold (GAMBIT) [50]). Equations and detailed explanations for these metrics are provided in Table 1. For example, PLA is used to predict the risk of skull fractures and focal brain injuries [65,66], and PAA has been proposed as a predictor for subdural hematoma (SDH) [67,68]. Given that these pathologies are commonly observed in VRU casualties, these metrics were employed to evaluate the head protection performance of the IAP and were post-processed using Python (v 3.12). Additionally, kernel density estimation was applied to visualize the distribution of peak strains across all elements during oblique impacts.

3. Results

3.1. Head injury metrics

Fig. 2 displays high-speed camera snapshots of five IAP samples tested at a drop height of 150 cm. The headform initiated rolling on the rubberized asphalt at approximately 3 ms and detached from the angled samples at around 15 ms. Under a given impact location, no significant differences in headform motion were visually observed among different asphalt types.

Fig. 3 illustrates a comparison of selected head injury metrics between the IAP and helmets with or without a rotational protection system (RPS) at 6.0 m/s oblique impacts, while all head injury metrics of IAP are illustrated in Fig. 4. IAP is comparable with helmets in oblique frontal impacts (Yrot), but slightly less protective than helmets in oblique side impacts (Xrot). The mean values and standard deviations for these metrics, calculated across five samples, are summarized in Table A.1. Overall, the IAP demonstrates the potential to effectively reduce the risk of severe head injuries. For example, the PLA across all impact cases averaged 114.89 ± 17.68 g, well below the 180 g threshold associated with a less than 5% risk of skull fracture [69]. The HIC value was 424.96 ± 146.44, remaining below the 700 threshold that suggests a low probability of severe brain injury (AIS 4+) [70]. As a reference, HIC of 1000 is equivalent to an 18% probability of a severe (AIS 4) head injury, a 55% likelihood of a serious (AIS 3) injury, and a 90% proba-

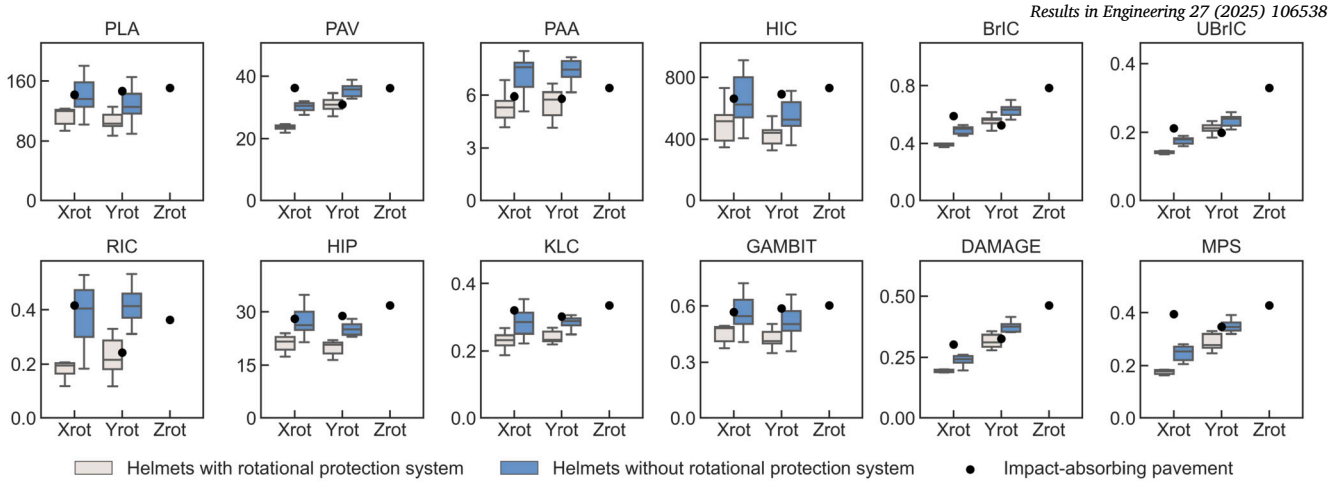

Fig. 3. Comparison of head injury metrics in oblique impacts at 6.0 m/s on Xrot and Yrot, between rubberized asphalt and helmets. The boxplots correspond to helmets data reported by previous studies [39,61], where the light yellow box represents the helmets with rotational protection system (RPS), while the light blue box represents the helmets without this technology. The black dots represent the metrics of impact-absorbing pavement. The Zrot was omitted because of the different impact positions. Notes that these datasets were obtained under different lab conditions.

bility of a moderate (AIS 2) head injury to the average adult [71]. The HIP was 20.22 ± 5.06 kW, also below the 48 kW threshold associated with a 50% probability of an AIS 5 injury based on real-world trauma cases [72].

Similarly, the PAV and PAA were 31.70 ± 2.87 rad/s and 5.26 ± 0.60 krad/s^2 respectively, both falling below the critical thresholds (46.5 rad/s and 16 krad/s^2) suggested for severe diffuse axonal injuries (DAI) [73,74]. However, certain metrics indicate a risk of mild traumatic brain injury (mTBI). For instance, the BrIC averaged 0.57 ± 0.09, which is near the 0.68 suggested threshold, corresponding to a 33% probability of concussion (AIS 2+) or a 5% probability of DAI (AIS 4+) based on scaling from animal experiments [75]. Additionally, GAMBIT of 0.46 ± 0.07 was close to 0.5, which represented a 5% risk of AIS 4+ brain injury [76]. At the brain tissue level, MPS was 0.34 ± 0.03, approaching the 36% risk level for mTBI [77].

IAP exhibited a pronounced increase in linear-based injury metrics with increasing impact velocity. For example, when the impact velocity rises from 5.4 m/s to 6.0 m/s, the metrics that include linear kinematics (PLA, HIC, HIP, KLC, and GAMBIT) showed increases of 34.78%, 88.14%, 63.38%, 39.18%, and 34.78%, respectively (in Fig. 4). In contrast, pure rotational-based metrics and strain-based metrics exhibited small variations across different asphalts or impact velocities. For E30 at 5.4 m/s and 6.0 m/s, the purely rotational-based metrics (PAV, PAA, BrIC, UBrIC, RIC, and DAMAGE) increased by 11.40%, 16.94%, 14.34%, 14.69%, 49.25%, and 14.42%, respectively. Similarly, the strain-based metrics (MPS, MTON, MTPN, MTOS, and MTPS) within brain tissues increased by 13.87%, 18.97%, 17.54%, 14.79%, and 11.69%, respectively (in Fig. 4). All the strain-based metrics were below 0.4, and the standard deviations remained below 0.04, suggesting that variations in impact velocity exerted only a minor influence on the head protection performance of the IAP. These findings suggest that while IAP can effectively reduce the severity of impacts, further optimizations are necessary to mitigate peak kinematics and brain strain.

3.2. Brain strain distribution

Fig. 5 exhibits the MPS distributions of brain tissues at three impact locations (Xrot, Yrot, and Zrot) during oblique impacts, while Fig. A.3 shows the tract-related strain distribution. Fig. 6 illustrates the MPS distributions of brain tissues in isometric, coronal, sagittal, and horizontal views between high-ranking (4-star) and low-ranking (1-star) helmets [39] and IAP (E30_2), respectively. The impact locations affected the brain strain peaks and their distribution. The oblique impact on Zrot caused a higher peak strain, followed by Xrot and Yrot. A large volume of the brain experienced an MPS of more than 0.3 in Zrot impact against all IAP samples, which produced large stains in the temporal lobes. Yrot impact produced large strains in the parietal lobe, while the Xrot impact only caused relatively lower strains across the brain. Similar trends were observed for tract-related strain distributions, where only a small volume of white matter underwent strains greater than 0.2. Oblique impacts against IAP led to relatively higher MTPN but lower MTPS among the tract-related strain metrics. Overall strain patterns at 6.0 m/s were comparable to those at 5.4 m/s.

The Pearson's correlation coefficient between strain-based metrics (MPS, MTON, MTPN, MTOS, MTPS) and kinematic-based metrics is shown in Fig. A.2. In general, the five strain-based metrics exhibited strong correlations (>0.7) with rotational-based metrics such as PAV, PAA, BrIC, UBrIC, and RIC. Exceptions included MTON with PAV, PAA, and RIC, as well as MTPS with BrIC and UBrIC, which showed comparatively weaker associations. In contrast, all five strains were correlated with the linear motion-related kinematics (e.g., PLA and HIC). In contrast, all strain-based metrics demonstrated only weak to moderate correlations with linear kinematic metrics such as PLA and HIC. These results are similar to the results reported by a previous study [61], and suggest that rotational kinematics are more strongly associated with strain-based injury metrics, which are indicative of brain injuries such as concussion.

The kernel density estimate and coefficient of determination (r^2) between element-wise MPS from different IAP samples are performed in Fig. 7, while those of four tract-related strains are illustrated in Fig. A.4. All r^2 values exceeded 0.98, indicating that variations in IAP configurations did not significantly affect the brain strain distribution. Additionally, there was no discernible difference between different IAP cycles (e.g., E30 vs. E80, EA30 vs. EA80) or between artificially aged samples (e.g., E30 vs. EA30, E80 vs. EA80), as evidenced by the density distribution in the kernel density estimate and the scatter dots closely following the $y = x$ line.

4. Discussion

This study biomechanically evaluated the head protective effectiveness of the IAP through oblique impacts. Five IAP samples were tested at three impact locations and two drop heights. Eleven kinematics-based and five strain-based head injury metrics were analyzed and compared.

An interesting observation was that the proposed IAP demonstrated head protection performance comparable to helmets. Several previous studies have assessed helmet performance through oblique impacts [78,79]. Specifically, Zhou et al. [61] and Fahlstedt et al. [39] tested 17

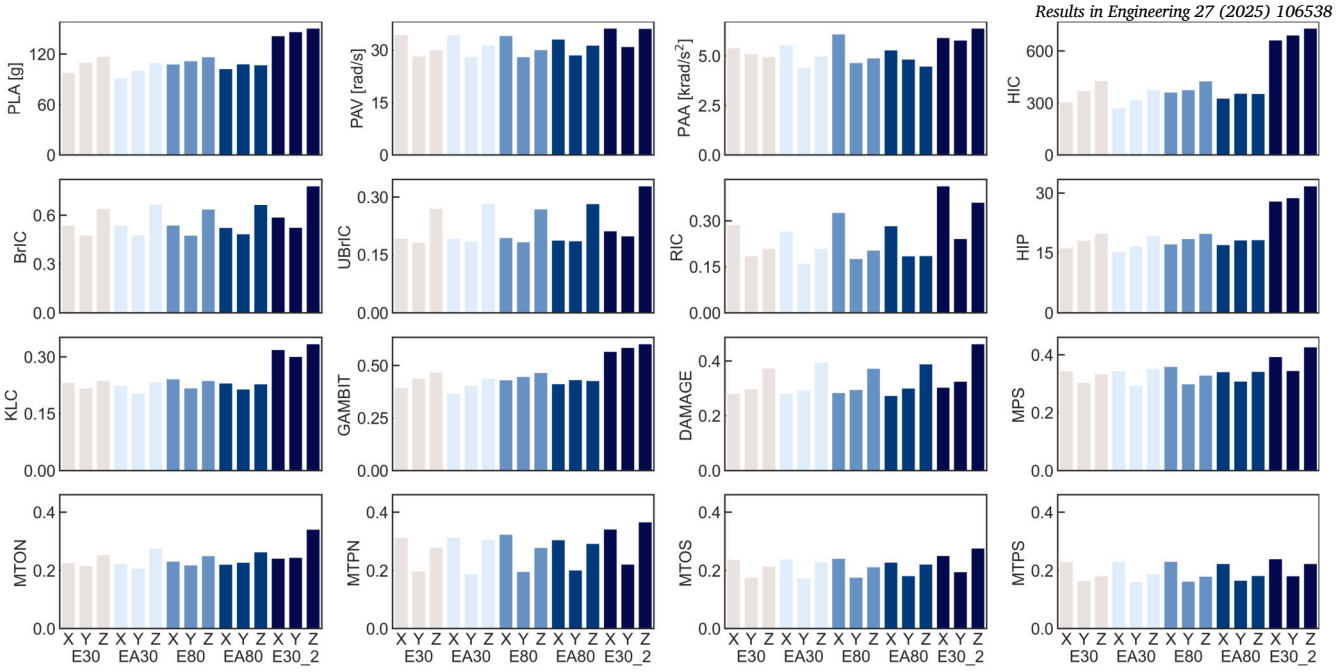

Fig. 4. Eleven kinematics-based and five strain-based head injury metrics of rubberized asphalt samples (E30, EA30, E80, and EA80) at three impact locations (Xrot, Yrot, and Zrot) at 5.4 m/s, where the E30_2 represented the E30 sample under the impact velocity at 6.0 m/s.

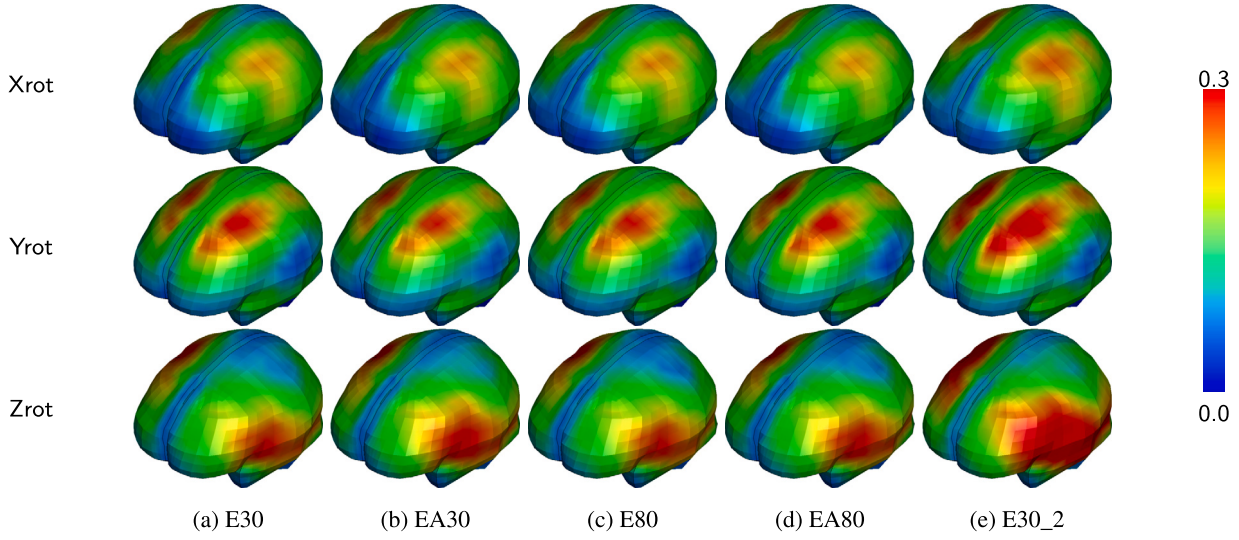

Fig. 5. Maximum principal strain (MPS) distribution of brain tissues during oblique impact against five asphalt samples at three impact locations (Xrot, Yrot, and Zrot), where the E30_2 represented the E30 sample under the impact velocity at 6.0 m/s. The color bar indicates strain from 0 to 0.3.

helmets at an impact velocity of 6.0 m/s across three impact directions, two of which (Xrot and Yrot) matched the experimental configurations used for evaluating the IAP E30 at the same velocity, thus enabling a direct performance comparison in Fig. 3. Generally, helmets equipped with RPS displayed lower values across all injury metrics than other helmets and the IAP. For linear-based injury metrics (e.g., PLA and HIC), values recorded for the IAP were slightly higher than the median values for helmets without RPS, yet remained below their maximum values. For purely rotational-based metrics (e.g., PAV, PAA, BrIC, UBrIC, RIC, and DAMAGE), the IAP values were even lower than the median values observed for helmets without RPS in Yrot. For metrics combining linear and angular motion (e.g., HIP, KLC, and GAMBIT), the IAP values were slightly above the mean values of the helmets, but still within a comparable range.

The head injury metrics for helmets and IAP were obtained under different conditions, so direct comparisons should be interpreted with caution. Although both oblique impacts used the same headform (HIII 50th percentile male), impact velocity (6.0 m/s), and angled anvil (45°), the contact conditions differ significantly. In helmet testing, the interface between the helmeted headform and the angled steel anvil is covered with 40-grit sandpaper, whereas in the IAP tests, there is direct contact between the bare headform and the IAP. The sandpaper was used on the metal anvil to replicate the realistic frictional interaction. In contrast, during the IAP tests, the rubberized asphalt surface itself already possesses frictional characteristics representative of real road surfaces; thus, no additional sandpaper is required. Previous studies [80,81] have highlighted the critical role of tangential forces in influencing rotational kinematics and brain injury. These tangential forces are proportional to both the coefficient of friction and the normal impact force. For example, Bonin et al. [82] demonstrated that the addition of HIII headform coverings, such as stockings or hair, can reduce peak rotational head kinematics. Similarly, Stark et al. [83] reported that rotational head

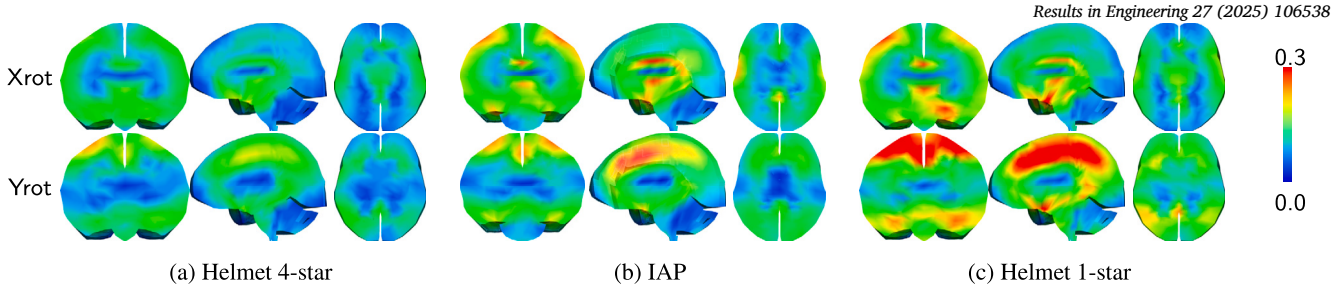

Fig. 6. MPS distribution of brain tissues in coronal, sagittal, and horizontal views for Xrot and Yrot. Zrot impacts between helmets and IAP were excluded due to differences in impact orientation. The suffixes "4-star" and "1-star" correspond to helmet ranking reported by previous studies [39]. The color bar indicates strain levels ranging from 0.0 to 0.3.

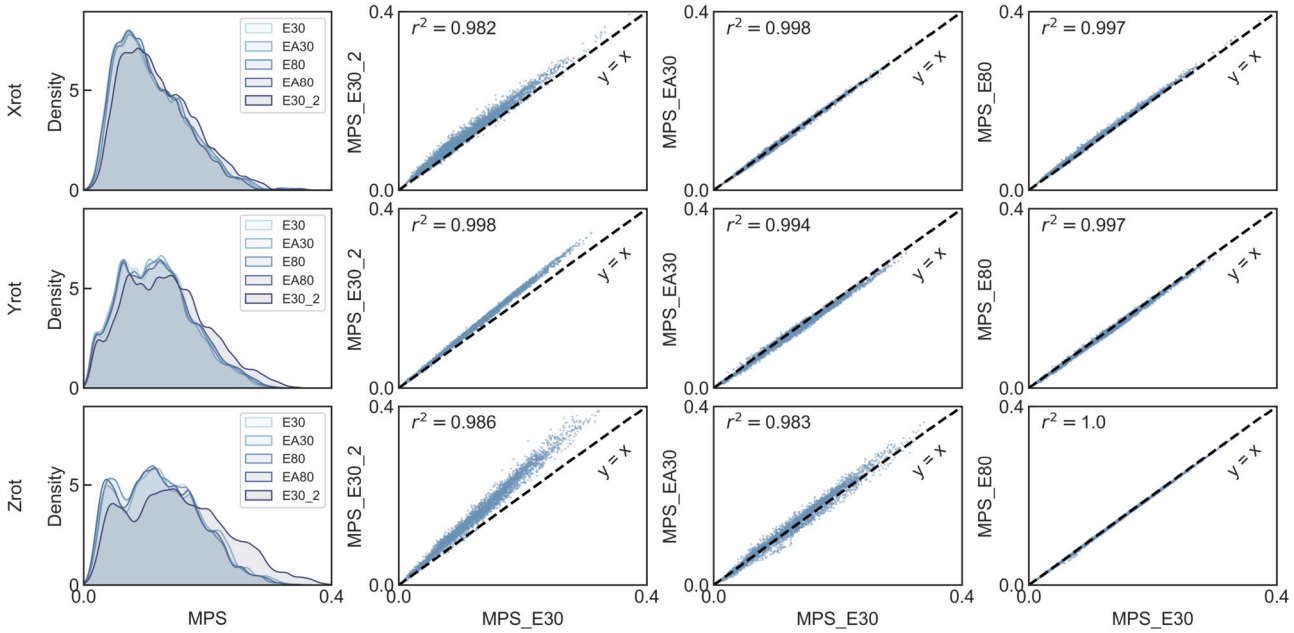

Fig. 7. The kernel density estimate and the coefficient of determination (r^2) between element-wise MPS from different rubberized asphalts during oblique tests at three impact locations (Xrot, Yrot, and Zrot), where the E30_2 represented the E30 sample under the impact velocity at 6.0 m/s. The four tract-related strains were illustrated in the Appendix.

kinematics are more sensitive to variations in inertial properties than to frictional differences, whereas linear kinematics are more affected by changes in frictional characteristics than by inertial parameters. The helmeted headform exhibits slightly higher inertia than the bare headform due to the additional mass of the helmet. The Zrot orientation was excluded in the comparison because of the different impact orientations. Previous studies [72] have shown that head injury metrics are highly dependent on the impact direction. Therefore, further research is necessary to compare the head protection performance at Zrot.

The newly developed IAP's ability to maintain low rotational acceleration and velocity is a significant breakthrough. Its rotational performance exhibits comparable head protection performance to helmets in identical testing scenarios, marking a substantial advancement in safety innovation. Additionally, the asphalt samples were fixed using a C-clamp during oblique impact testing, and their dimensions were constrained by the U-shaped free-falling trolley. This setup introduced an idealized boundary condition that restricted the lateral displacement and shear deformation of the rubberized asphalt. However, IAP would likely undergo greater lateral motion and shear in real-world scenarios, which has the potential to increase energy absorption further and reduce peak kinematics. It indicated that IAP may achieve higher head protection performance in practical applications than in laboratory experiments. Further studies are needed to validate this assumption and to better understand the performance of head protection. The combination of both IAP and helmet use holds significant potential for enhancing head protection for VRUs. While helmets are designed to absorb impact energy and reduce the severity of head injuries, pavement characteristics can also play a role in mitigating injury. Pavement, as a collective form of protection, can benefit all users, including those who do not wear helmets. However, it is important to approach this combination with caution, as previous studies have shown that while helmet use combined with softer surfaces may reduce skull fractures, it can have a counterintuitive effect on the brain tissue, possibly due to the increased contact area and contact time [20]. Therefore, while the potential synergy between helmet use and improved pavement materials seems promising, further research is needed to fully understand the synergy effect.

The 56% volume value of rubber aligns with previous laboratory trials aimed at determining an optimal threshold that balances injury reduction performance with maintaining sufficient structural resistance. Since the material is intended for an outdoor path and must withstand loads, even if limited to pedestrians or lightweight vehicles, this balance is crucial. As the number of gyratory compaction cycles increases, the samples become more compacted, reducing the space available for air voids [84] and consequently decreasing air-related attenuation. Comparing the material at 30 and 80 cycles, both identified as relevant from a material cohesion perspective, was essential to understanding the influence of compaction on injury reduction properties. Additionally, the

aging of asphalt materials over a full life cycle in outdoor conditions tends to increase the hardening process, thus the stiffness of the material [85,86]. The tested materials appeared stiffer on the surface compared to the non-aged ones, highlighting the necessity of evaluating aged samples for injury performance to assess the potential evolution of their properties. However, since the laboratory procedure was simplified by considering only restricted heat and UV exposure, the results may not fully capture the complexity of real in-situ aging conditions, introducing a source of uncertainty in the results. Even though these two mentioned parameters, the compaction level and the aging, are well known to influence the material itself, in the studied form, they did not result in significantly different values in terms of impact-absorbing performance.

The incorporation of recycled tire rubber and the demonstrated injury reduction capabilities position this material as a valuable asset in supporting communities' efforts toward more responsible consumption and adherence to circular economy principles. Additionally, its performance aligns with developing more sustainable cities and communities [87]. Ongoing research is focused on optimizing the performance of IAP by refining mix designs and improving its mechanical properties to ensure durability and effectiveness under various environmental conditions. By rethinking traditional pavement materials and designs, IAP is prepared to contribute significantly to the development of safer, more sustainable cities. Some studies have argued that the use of personal protective equipment may lead to increased risk-taking behavior due to a perceived sense of safety [88–90]. Although this study did not investigate behavioral responses of pavement users, the goal of IAP is to provide passive protection that enhances overall safety, regardless of individual behavior or equipment usage. Nevertheless, continued research and innovation in IAP design and injury biomechanics are essential to fully realize its protective potential, ensure broader applicability across diverse user groups, and support its long-term implementation in real-world traffic environments. In particular, coupling experimental findings with a broader set of real-world accident data and clinical records will enhance the translational relevance of IAP-related safety assessments.

Although the current study focuses on controlled laboratory impact scenarios, the real-world implementation of IAP introduces additional complexities. In practical applications, the IAP layer is designed to replace the upper portion of existing pavement systems—typically the surface and, in some cases, the binder course—while leaving the subbase and base layers intact. Preliminary installations in both Sweden [9] and Italy [17] have demonstrated that the IAP adheres well to traditional base layers without compromising structural integrity. However, interfacial bonding remains a critical factor in ensuring long-term performance, particularly in layered pavement systems. Future studies could further explore the structural effects of integrating IAP with diverse sub-layer compositions and construction methods. Environmental factors also play an important role in IAP performance and durability. Although the rubberized component offers certain advantages in terms of resilience, exposure to UV radiation, temperature extremes, snow accumulation, and freeze–thaw cycles can influence material aging and impact-absorbing behavior. Previous complementary laboratory simulations [10,18] have also been carried out to assess performance under freeze–thaw cycles and high-temperature/UV exposure, suggesting that the IAP retains its protection performance under a range of environmental stressors. Continued formulation refinements—such as tuning rubber content and enhancing binder properties—are necessary to optimize both safety and longevity across diverse geographic regions. Furthermore, real-world pavements often exhibit surface irregularities and curvature that differ from the idealized test conditions used in the current setup. Although the samples used here were fabricated via standard laboratory compaction protocols to capture representative surface textures, they were flat and uniformly constrained. Future testing with large-scale, curved, or semi-free samples may better reflect field conditions such as road camber or embedded surface defects, and help validate the robustness of the observed protective performance under more realistic geometries. Collectively, these considerations highlight the importance of further translational research to bridge the gap between controlled laboratory validation and real-world performance.

This study has some limitations that should be clarified. First, only one IAP sample at 6.0 m/s was included for each impact location, which may not accurately represent the average performance of IAP. This choice was based on the observed consistency in IAP performance at 5.4 m/s, so we assumed that the aging and cycling processes of rubberized asphalt would not affect head protection performance. The circumferential boundary conditions of the asphalt were not considered in the experiments. Future work will include testing more IAP samples at various impact velocities and under different initial conditions. Second, the oblique impact tests employed a HIII headform in its bare configuration. Although this headform is widely used, its biofidelity is limited (such as moments of inertia and coefficient of friction) compared to human head properties [91,92], which may influence the accuracy of head kinematics during impact. The newly developed headform with high biofidelity (e.g., EN17950 with adapted mass moments and realistic friction characteristics) will be considered in the future evaluation study. Third, the comparative analysis of head protection efficacy between asphalt and helmets was conducted under different test conditions. For instance, there is no sandpaper covering the IAP surface, and different head models also introduced variability. Direct comparisons of strain distribution outcomes should be interpreted with caution. The synergy effect that combines helmets and IAP also remains to be investigated. Fourth, to the best of our knowledge, only two studies [62,93] have computed in vivo DTI-based strain fields. Both studies were performed based on an open-access dataset [94]. Despite their availability, these data are measured from impact loading far from the injury level, and we tend to think they are less relevant for the validation of a head model with intended usage for injury prediction. Further research is necessary to improve the applicability and generalization of these findings.

5. Conclusion

This study biomechanically evaluated the head protection performance of the impact-absorbing pavement through oblique impacts. A total of 30 impact tests were performed on five kinds of asphalt samples under three impact orientations, with each test repeated twice. Sixteen head injury metrics were analyzed and compared.

The results demonstrated that the proposed IAP effectively reduces both peak linear and rotational head kinematics and substantially reduces the risk of severe head injuries, even achieving a comparable head protection performance to helmets. These findings indicate that IAP has significant potential to reduce head injuries among unprotected VRUs and contribute to safer traffic environments.

CRediT authorship contribution statement

Christina Makoundou: Writing – original draft, Resources, Methodology, Investigation, Conceptualization. **Qi Huang:** Writing – original draft, Validation, Software, Methodology, Formal analysis, Data curation. **Chengbin Li:** Software, Formal analysis. **Zhou Zhou:** Writing – review & editing, Validation, Software. **Svein Kleiven:** Writing – review & editing, Supervision, Funding acquisition. **Cesare Sangiorgi:** Writing – review & editing, Supervision, Project administration, Funding acquisition.

Declaration of competing interest

The authors declare that they have no known competing financial interests or personal relationships that could have appeared to influence the work reported in this paper.

Acknowledgements

The core of this study was funded by the European Union's Horizon 2020 research and innovation program under the Marie Skłodowska-Curie grant agreement [no. 765057] through the SAFERUP! Project. This work was also supported by the Swedish Governmental Agency for Innovation Systems (Vinnova) [no. 2021-01598] and Skyltfonden [no. 2024-107146, 2024-106547, and 2025-27050]. The simulations were enabled by resources in projects [NAISS 2025/5-122, 2025/5-147, and 2024/5-668] provided by the National Academic Infrastructure for Supercomputing in Sweden (NAISS), partially funded by the Swedish Research Council through the grant agreement [no. 2022-06725]. The open-access funding was provided by the KTH Royal Institute of Technology.

The authors would like to express sincere gratitude to Ing. Filippo Venturucci for assistance in facilitating part of this study, Dr. Madelen Fahlstedt for her valuable help with oblique impact testing and insightful discussions, Dr. Yuqi Zheng for her thoughtful insights in data visualization, Folksam (Sweden) for generously providing bicycle helmet test data, and the materials supplier whose products were utilized throughout this research.

Appendix A

In the appendix, we list the summary of sixteen head injury metrics of all rubberized asphalt (Table A.1), the kinematics of each oblique test extracted from the HIII headform (Fig. A.1), Pearson's correlation coefficient between strain-based metrics and kinematic-based metrics (Fig. A.2), tract-related strain distributions during oblique impacts in the FE simulations (Fig. A.3), and the coefficient of determination (r^2) between element-wise tract-related strain (Fig. A.4).

Table A.1
Summary of sixteen head injury metrics of all rubberized asphalts in the form of mean ± standard deviation at three impact locations (Xrot, Yrot, and Zrot) and two drop heights (150 cm and 205 cm).

	PLA	PAV	PAA	HIC	BrIC	UBrIC	RIC	HIP
Xrot	108.60 ± 19.51	34.45 ± 1.12	5.66 ± 0.34	386.84 ± 158.12	0.55 ± 0.02	0.19 ± 0.01	0.32 ± 0.06	18.75 ± 5.24
Yrot	115.63 ± 17.84	28.83 ± 1.23	4.97 ± 0.53	423.38 ± 151.67	0.49 ± 0.02	0.19 ± 0.01	0.19 ± 0.03	20.08 ± 4.96
Zrot	120.44 ± 17.51	31.83 ± 2.51	5.15 ± 0.73	464.67 ± 152.49	0.68 ± 0.06	0.29 ± 0.03	0.23 ± 0.07	21.84 ± 5.62

	KLC	GAMBIT	DAMAGE	MPS	MTON	MTPN	MTOS	MTPS
Xrot	0.25 ± 0.04	0.43 ± 0.08	0.28 ± 0.01	0.35 ± 0.01	0.23 ± 0.01	0.32 ± 0.01	0.24 ± 0.01	0.23 ± 0.01
Yrot	0.23 ± 0.04	0.46 ± 0.07	0.30 ± 0.02	0.31 ± 0.02	0.23 ± 0.02	0.20 ± 0.01	0.18 ± 0.01	0.17 ± 0.01
Zrot	0.25 ± 0.05	0.48 ± 0.07	0.40 ± 0.04	0.35 ± 0.04	0.28 ± 0.04	0.31 ± 0.04	0.23 ± 0.03	0.19 ± 0.02

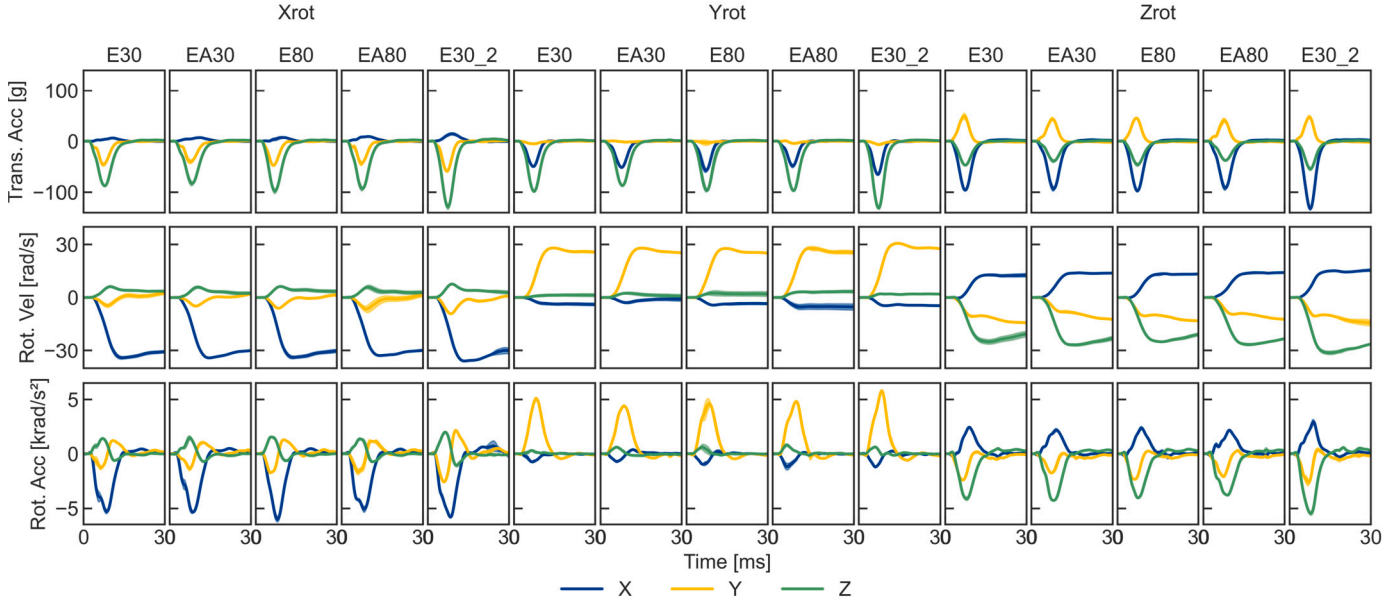

Fig. A.1. Kinematics including linear acceleration, angular velocity, and angular acceleration of 30 oblique impacts extracted from the HIII headform. Five kinds of rubberized asphalt samples under three impact locations (Xrot, Yrot, and Zrot), each test repeated twice. The solid curve in each sub-figure represents the average kinematics, while the filled region bounds the minimum and maximum recorded kinematics of the repeats.

	PLA	PAV	PAA	HIC	BrIC	UBrIC	RIC	HIP	KLC	GAMBIT	DAMAGE
MPS	0.62	0.89	0.81	0.67	0.73	0.57	0.86	0.69	0.85	0.62	0.51
MTON	0.63	0.44	0.43	0.63	0.93	0.91	0.36	0.68	0.66	0.63	0.92
MTPN	0.22	0.92	0.65	0.27	0.69	0.52	0.79	0.29	0.54	0.22	0.36
MTOS	0.30	0.95	0.72	0.35	0.70	0.52	0.83	0.38	0.61	0.30	0.38
MTPS	0.11	0.96	0.77	0.19	0.28	0.05	0.90	0.19	0.48	0.11	-0.10

Fig. A.2. Pearson's correlation coefficient between five strain-based metrics and eleven kinematic-based metrics, with strong correlations (>0.7) indicated in dark blue.

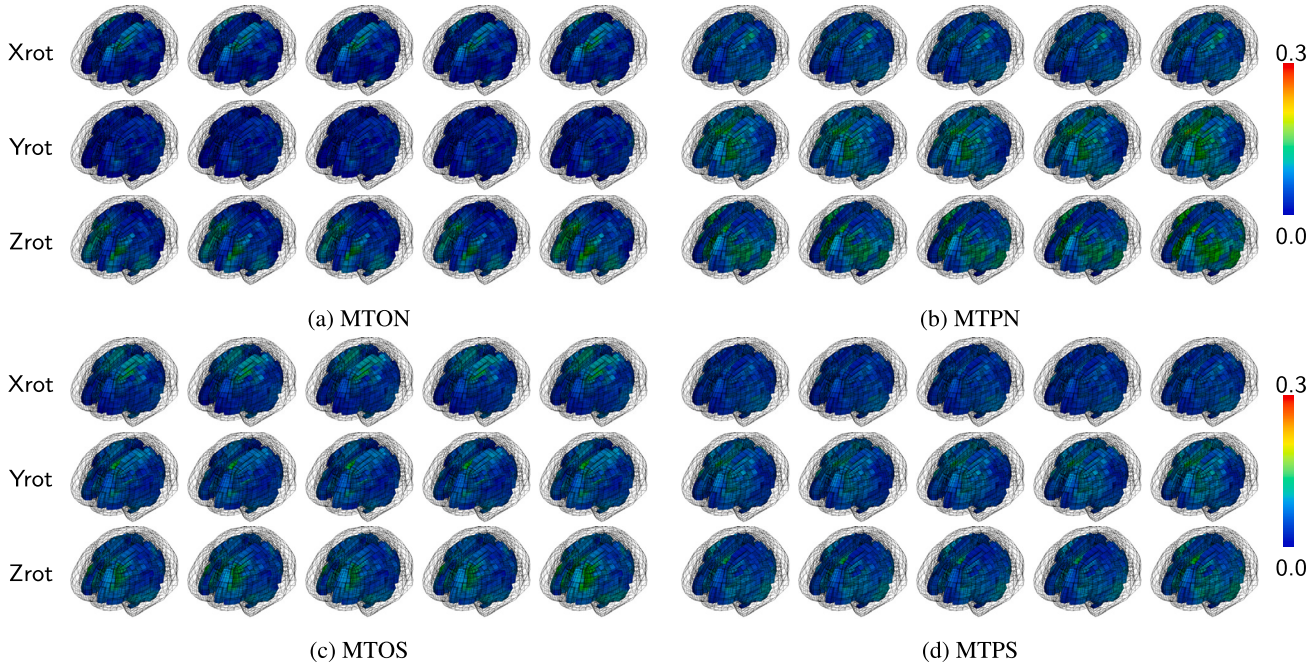

Fig. A.3. Four tract-related strain distribution of white matter during oblique impacts at three impact locations (Xrot, Yrot, and Zrot). From left to right are five IAP samples: E30, EA30, E8, EA80, and E30_2, respectively. Part of the brain tissues in the subfigures were rendered transparent to visualize the white matter. The color bar indicates strain from 0 to 0.3.

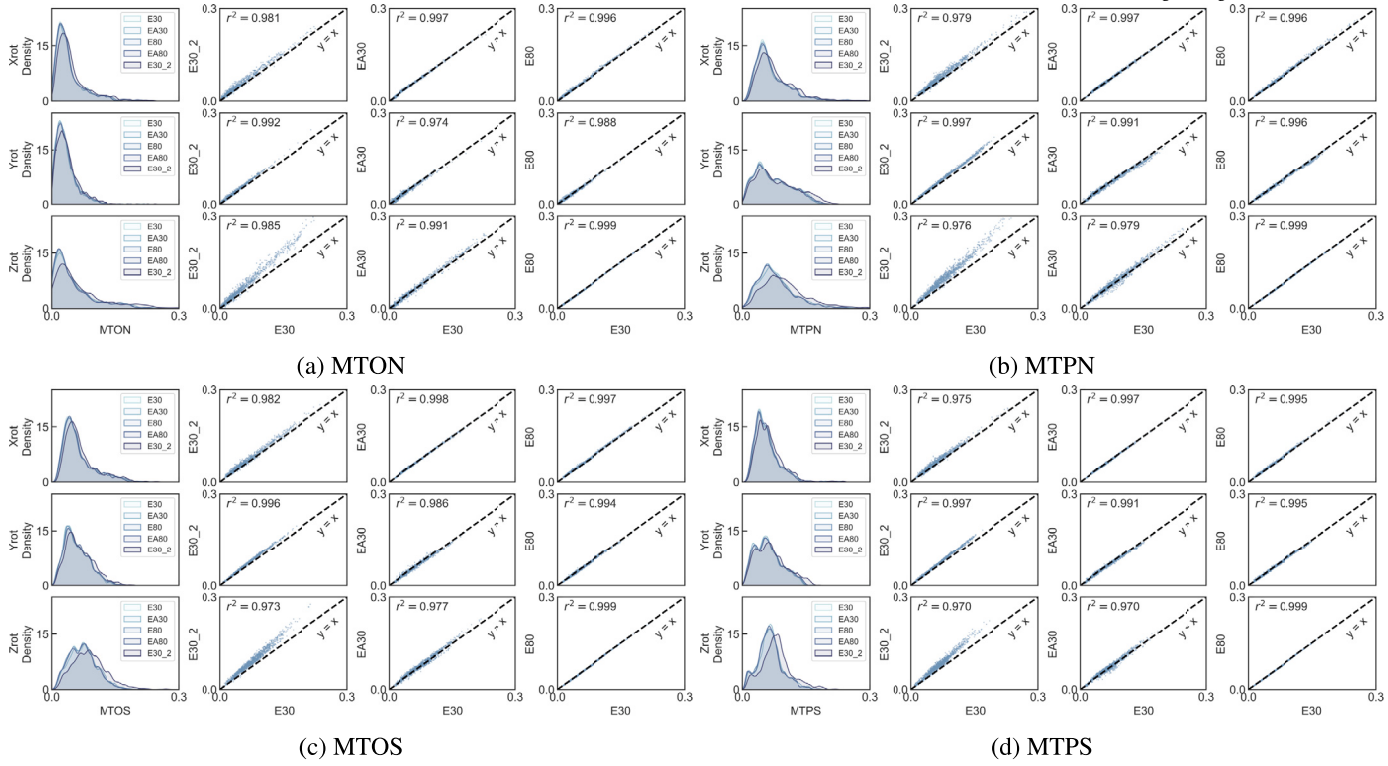

Fig. A.4. The kernel density estimate and the coefficient of determination (r^2) between element-wise tract-related strain from different rubberized asphalts during oblique tests at three impact locations (Xrot, Yrot, and Zrot), where the E30_2 represented the E30 sample under the impact velocity at 6.0 m/s.

Data availability

Data will be made available on request.

References

[1] P. Hurtig, P. Larsson, M. Lindholm, M. Rizzi, S. Sternlund, A.-L. Elmqvist, R. Fredriksson, Å. Forsman, A. Vadeby, K. Amin, Analysis of Road Safety Trends 2022: Management by Objectives for Road Safety Work Towards the 2030 Interim Targets, 2023.

[2] T. Stewart, et al., Overview of motor vehicle traffic crashes in 2021, Tech. Rep., U.S. Department of Transportation, National Highway Traffic Safety …, 2023.

[3] K. Brookshire, W. Kumfer, A. West, L. Thomas, B. Judelman, F. Proulx, M. Hintze, et al., Pedestrian and bicyclist safety–literature review, Tech. Rep., U.S. Department of Transportation, National Highway Traffic Safety Administration, 2025.

[4] I. Isaksson-Hellman, M. Lindman, Real-world evaluation of driver assistance systems for vulnerable road users based on insurance crash data in Sweden, in: The 26th ESV Conference Proceedings, NHTSA Washington, DC, 2019.

[5] D. Piatkowski, M. Bopp, Increasing bicycling for transportation: a systematic review of the literature, J. Urban Plann. Dev. 147 (2) (2021) 04021019.

[6] I. Næss, P. Galteland, N.O. Skaga, T. Eken, E. Helseth, J. Ramm-Pettersen, The number of patients hospitalized with bicycle injuries is increasing-a cry for better road safety, Accid. Anal. Prev. 148 (2020) 105836.

[7] M. Fahlstedt, P. Halldin, S. Kleiven, The protective effect of a helmet in three bicycle accidents—a finite element study, Accid. Anal. Prev. 91 (2016) 135–143.

[8] C. Makoundou, C. Sangiorgi, K. Johansson, V. Wallqvist, Development of functional rubber-based impact-absorbing pavements for cyclist and pedestrian injury reduction, Sustainability 13 (20) (2021) 11283.

[9] V. Wallqvist, L. Kraft, Prototype bike lanes-placement practices and properties, in: Proceedings of the 3rd International Conference on Best Practices for Concrete Pavements, Bonito, Brazil, 2015, pp. 28–30.

[10] C. Makoundou, A. Fathollahi, S. Kleiven, S.J. Coupe, C. Sangiorgi, Mechanical and leaching characterisation of impact-absorbing rubberised asphalts for urban pavements, Mater. Struct. 56 (3) (2023) 55.

[11] D.L. Presti, Recycled tyre rubber modified bitumens for road asphalt mixtures: a literature review, Constr. Build. Mater. 49 (2013) 863–881.

[12] M. Fahlstedt, S. Kleiven, X. Li, Current playground surface test standards underestimate brain injury risk for children, J. Biomech. 89 (2019) 1–10.

[13] G.N. Viktorovich, A. Almusawi, S. Shoman, A.P. Lupanov, M. Albdairi, Integrating recycled asphalt pavement and warm mix additives for enhanced performance and reduced emissions in asphalt mixtures, Results Eng. 26 (2025) 104754.

[14] D. Shirvani, A. Sarkar, Technical evaluation of using reclaimed asphalt pavement materials as filler in hot mix asphalt, Results Eng. (2025) 106048.

[15] V. Vijayan, E. Manthos, K. Mantalovas, G. Di Mino, Multi-recyclability of asphalt mixtures modified with recycled plastic: towards a circular economy, Results Eng. 23 (2024) 102523.

[16] X. Li, S. Kleiven, Improved safety standards are needed to better protect younger children at playgrounds, Sci. Rep. 8 (1) (2018) 15061.

[17] C. Makoundou, K. Johansson, V. Wallqvist, C. Sangiorgi, Rubber- and emulsion-based impact-absorbing paving material produced with cold and dry processes: laboratory and in-situ study, Constr. Build. Mater. 408 (2023) 133496.

[18] C. Makoundou, C. Sangiorgi, Influence of freeze–thaw cycles on the mechanical properties of highly rubberised asphalt mixtures made with warm and cold asphalt binders, Materials 15 (7) (2022) 2701.

[19] P. Sahandifar, V. Wallqvist, S. Kleiven, Assessing the impact of rubberized asphalt on reducing hip fracture risk in elderly populations using human body models, SAE Int. J. Transp. Saf. 12 (o) (2024) 09.

[20] P. Sahandifar, C. Makoundou, M. Fahlstedt, C. Sangiorgi, K. Johansson, V. Wallqvist, S. Kleiven, A rubberized impact absorbing pavement can reduce the head injury risk in vulnerable road users: a bicycle and a pedestrian accident case study, Traffic Inj. Prev. 23 (5) (2022) 315–320.

[21] M.L. Bland, C. McNally, J.B. Cicchino, D.S. Zuby, B.C. Mueller, M.L. McCarthy, C.D. Newgard, P.E. Kulie, B.N. Arnold, S. Rowson, Laboratory reconstructions of bicycle helmet damage: investigation of cyclist head impacts using oblique impacts and computed tomography, Ann. Biomed. Eng. 48 (2020) 2783–2795.

[22] A.S. McIntosh, A. Lai, E. Schilter, Bicycle helmets: head impact dynamics in helmeted and unhelmeted oblique impact tests, Traffic Inj. Prev. 14 (5) (2013) 501–508.

[23] A.I. King, K.H. Yang, L. Zhang, W. Hardy, D.C. Viano, Is head injury caused by linear or angular acceleration, in: IRCOBI Conference, Lisbon, Portugal, vol. 12, 2003.

[24] A. Post, T. Blaine Hoshizaki, Rotational acceleration, brain tissue strain, and the relationship to concussion, J. Biomech. Eng. 137 (3) (2015) 030801.

[25] M. Ghajari, S. Peldschus, U. Galvanetto, L. Iannucci, Effects of the presence of the body in helmet oblique impacts, Accid. Anal. Prev. 50 (2013) 263–271.

[26] M.L. Bland, C. McNally, D.S. Zuby, B.C. Mueller, S. Rowson, Development of the star evaluation system for assessing bicycle helmet protective performance, Ann. Biomed. Eng. 48 (1) (2020) 47–57.

[27] P. Halldin, A. Gilchrist, N. Mills, A new oblique impact test for motorcycle helmets, Int. J. Crashworthiness 6 (1) (2001) 53–64.

[28] C. Klug, F. Feist, E. Tomasch, Testing of bicycle helmets for preadolescents, in: International Research Council on the Biomechanics of Injury (IRCOBI), Lyon, France, 2015, pp. 136–155.

[29] M. Fahlstedt, P. Halldin, V.S. Alvarez, S. Kleiven, Influence of the body and neck on head kinematics and brain injury risk in bicycle accident situations, in: IRCOBI 2016, International Research Council on the Biomechanics of Injury, 2016, pp. 459–478.
[30] A. Bartsch, E. Benzel, V. Miele, D. Morr, V. Prakash, Hybrid iii anthropomorphic test device (atd) response to head impacts and potential implications for athletic headgear testing, Accid. Anal. Prev. 48 (2012) 285–291.
[31] X. Yu, M. Ghajari, Protective performance of helmets and goggles in mitigating brain biomechanical response to primary blast exposure, Ann. Biomed. Eng. 50 (11) (2022) 1579–1595.
[32] X. Yu, I. Logan, I. de Pedro Sarasola, A. Dasaratha, M. Ghajari, The protective performance of modern motorcycle helmets under oblique impacts, Ann. Biomed. Eng. 50 (11) (2022) 1674–1688.
[33] Q. Huang, Z. Zhou, S. Kleiven, Deep learning-augmented biomechanical optimization of energy-absorbing structure towards improved hip injury protection, Knowl.-Based Syst. (2025) 113979.
[34] X. Zhan, Y. Liu, S.J. Raymond, H.V. Alizadeh, A.G. Domel, O. Gevaert, M.M. Zeineh, G.A. Grant, D.B. Camarillo, Rapid estimation of entire brain strain using deep learning models, IEEE Trans. Biomed. Eng. 68 (11) (2021) 3424–3434.
[35] X. Zhan, Y. Liu, N.J. Cecchi, O. Gevaert, M.M. Zeineh, G.A. Grant, D.B. Camarillo, Brain deformation estimation with transfer learning for head impact datasets across impact types, IEEE Trans. Biomed. Eng. 71 (6) (2024) 1853–1863.
[36] D. Xu, H. Zhou, T. Jie, Z. Zhou, Y. Yuan, M. Jemni, W. Quan, Z. Gao, L. Xiang, F. Gusztav, et al., Data-driven deep learning for predicting ligament fatigue failure risk mechanisms, Int. J. Mech. Sci. (2025) 110519.
[37] P. Halldin, S. Kleiven, The development of next generation test standards for helmets, in: 1st International Conference on Helmet Performance and Design, vol. 1, 2013.
[38] P. Halldin, M. Aare, S. Kleiven, H. von Holst, Improved helmet design and test methods to reduce rotational induced brain injuries, in: RTO Specialist Meeting, the NATO's Research and Technology Organization (RTO), 2003.
[39] M. Fahlstedt, F. Abayazid, M.B. Panzer, A. Trotta, W. Zhao, M. Ghajari, M.D. Gilchrist, S. Ji, S. Kleiven, X. Li, et al., Ranking and rating bicycle helmet safety performance in oblique impacts using eight different brain injury models, Ann. Biomed. Eng. 49 (2021) 1097–1109.
[40] M. Arnesen, S. Hallström, P. Halldin, A. Kulachenko, A comparative study of constitutive models for eps foam under combined compression and shear impact loading for helmet applications, Results Eng. 23 (2024) 102685.
[41] E. C. for Standardization (CEN), EN 1078:2012+A1:2012 - Helmets for Pedal Cyclists and for Users of Skateboards and Roller Skates, 2012.
[42] E. C. for Standardization (CEN), CEN/TC 158 - WG11 Rotational Test Methods, European Committee for Standardization, 2014.
[43] A.J. Padgaonkar, K. Krieger, A. King, Measurement of angular acceleration of a rigid body using linear accelerometers, J. Appl. Mech. 42 (1975) 552–556.
[44] J. Versace, A review of the severity index, SAE Technical Paper, 1971.
[45] E.G. Takhounts, M.J. Craig, K. Moorhouse, J. McFadden, V. Hasija, Development of brain injury criteria (bric), Tech. Rep., SAE Technical Paper, 2013.
[46] L.F. Gabler, J.R. Crandall, M.B. Panzer, Development of a metric for predicting brain strain responses using head kinematics, Ann. Biomed. Eng. 46 (2018) 972–985.
[47] H. Kimpara, M. Iwamoto, Mild traumatic brain injury predictors based on angular accelerations during impacts, Ann. Biomed. Eng. 40 (2012) 114–126.
[48] J.A. Newman, N. Shewchenko, A proposed new biomechanical head injury assessment function-the maximum power index, Tech. Rep., SAE Technical Paper, 2000.
[49] S. Kleiven, Predictors for traumatic brain injuries evaluated through accident reconstructions, Tech. Rep., SAE Technical Paper, 2007.
[50] J.A. Newman, A generalized acceleration model for brain injury threshold (gambit), in: Proceedings of International Conference on the Biomechanics of Impact, 1986, 1986, pp. 121–131.
[51] L.F. Gabler, J.R. Crandall, M.B. Panzer, Development of a second-order system for rapid estimation of maximum brain strain, Ann. Biomed. Eng. 47 (2019) 1971–1981.
[52] Z. Zhou, T. Wang, D. Jörgens, X. Li, Fiber orientation downsampling compromises the computation of white matter tract-related deformation, J. Mech. Behav. Biomed. Mater. 132 (2022) 105294.
[53] Z. Zhou, X. Li, Y. Liu, M. Fahlstedt, M. Georgiadis, X. Zhan, S.J. Raymond, G. Grant, S. Kleiven, D. Camarillo, et al., Toward a comprehensive delineation of white matter tract-related deformation, J. Neurotrauma 38 (23) (2021) 3260–3278.
[54] S. Kleiven, W.N. Hardy, Correlation of an fe model of the human head with local brain motion-consequences for injury prediction, Tech. Rep., SAE Technical Paper, 2002.
[55] C. Giordano, S. Kleiven, Development of an unbiased validation protocol to assess the biofidelity of finite element head models used in prediction of traumatic brain injury, Tech. Rep., SAE Technical Paper, 2016.
[56] S. Kleiven, Evaluation of head injury criteria using a finite element model validated against experiments on localized brain motion, intracerebral acceleration, and intracranial pressure, Int. J. Crashworthiness 11 (1) (2006) 65–79.
[57] Z. Zhou, X. Li, S. Kleiven, Biomechanics of periventricular injury, J. Neurotrauma (2020).
[58] Q. Huang, S. Kleiven, Finite element analysis of energy-absorbing floors for reducing head injury risk during fall accidents, Appl. Sci. 13 (24) (2023) 13260.
[59] Q. Huang, Z. Zhou, S. Kleiven, Effectiveness of energy absorbing floors in reducing hip fractures risk among elderly women during sideways falls, J. Mech. Behav. Biomed. Mater. 157 (2024) 106659.
[60] Q. Huang, N. Lindgren, Z. Zhou, X. Li, S. Kleiven, A method for generating case-specific vehicle models from a single-view vehicle image for accurate pedestrian injury reconstructions, Accid. Anal. Prev. 200 (2024) 107555.
[61] Z. Zhou, M. Fahlstedt, X. Li, S. Kleiven, Peaks and distributions of white matter tract-related strains in bicycle helmeted impacts: implication for helmet ranking and optimization, Ann. Biomed. Eng. (2024) 1–19.
[62] Z. Zhou, C. Olsson, T.C. Gasser, X. Li, S. Kleiven, The white matter fiber tract deforms most in the perpendicular direction during in vivo volunteer impacts, J. Neurotrauma 41 (23–24) (2024) 2554–2570.
[63] Z. Zhou, X. Li, A.G. Domel, E.L. Dennis, M. Georgiadis, Y. Liu, S.J. Raymond, G. Grant, S. Kleiven, D. Camarillo, et al., The presence of the temporal horn exacerbates the vulnerability of hippocampus during head impacts, Front. Bioeng. Biotechnol. 10 (2022) 754344.
[64] X. Zhan, Y. Li, Y. Liu, A.G. Domel, H.V. Alizadeh, S.J. Raymond, J. Ruan, S. Barbat, S. Tiernan, O. Gevaert, et al., The relationship between brain injury criteria and brain strain across different types of head impacts can be different, J. R. Soc. Interface 18 (179) (2021) 20210260.
[65] D.L. Allsop, C.Y. Warner, M.G. Wille, D.C. Schneider, A.M. Nahum, Facial impact response—a comparison of the hybrid iii dummy and human cadaver, SAE Transact. (1988) 1224–1240.
[66] E.S. Gurdjian, V. Roberts, L.M. Thomas, Tolerance curves of acceleration and intracranial pressure and protective index in experimental head injury, J. Trauma Acute Care Surg. 6 (5) (1966) 600–604.
[67] B. Depreitere, C. Van Lierde, J. Vander Sloten, R. Van Audekercke, G. Van Der Perre, C. Plets, J. Goffin, Mechanics of acute subdural hematomas resulting from bridging vein rupture, J. Neurosurg. 104 (6) (2006) 950–956.
[68] T.A. Gennarelli, L.E. Thibault, Biomechanics of acute subdural hematoma, J. Trauma Acute Care Surg. 22 (8) (1982) 680–686.
[69] H.J. Mertz, P. Prasad, G. Nusholtz, Head injury risk assessment for forehead impacts, SAE Transact. (1996) 26–46.
[70] H.J. Mertz, P. Prasad, A.L. Irwin, Injury risk curves for children and adults in frontal and rear collisions, SAE Transact. (1997) 3563–3580.
[71] M. Mackay, The increasing importance of the biomechanics of impact trauma, Sadhana 32 (4) (2007) 397–408.
[72] S. Kleiven, Influence of impact direction on the human head in prediction of subdural hematoma, J. Neurotrauma 20 (4) (2003) 365–379.
[73] A.K. Ommaya, Biomechanics of head injuries: experimental aspects, Biomech. Trauma (1984).
[74] S.S. Margulies, L.E. Thibault, A proposed tolerance criterion for diffuse axonal injury in man, J. Biomech. 25 (8) (1992) 917–923.
[75] E.G. Takhounts, V. Hasija, S.A. Ridella, S. Rowson, S.M. Duma, Kinematic rotational brain injury criterion (BRIC), in: Proceedings of the 22nd Enhanced Safety of Vehicles Conference, in: Conference Proceedings, 2011, 11-0263.
[76] J. Newman, M. Beusenberg, E. Fournier, N. Shewchenko, C. Withnall, A. King, K. Yang, L. Zhang, J. McElhaney, L. Thibault, et al., A new biomechanical assessment of mild traumatic brain injury–part 1–methodology, in: Proceedings of the International Research Conference on the Biomechanics of Impacts (IRCOBI), Montpellier Sitges, 1999, pp. 17–36.
[77] M. Fahlstedt, S. Meng, S. Kleiven, Influence of strain post-processing on brain injury prediction, J. Biomech. 132 (2022) 110940.
[78] F. Abayazid, K. Ding, K. Zimmerman, H. Stigson, M. Ghajari, A new assessment of bicycle helmets: the brain injury mitigation effects of new technologies in oblique impacts, Ann. Biomed. Eng. 49 (10) (2021) 2716–2733.
[79] X. Yu, P. Halldin, M. Ghajari, Oblique impact responses of hybrid iii and a new headform with more biofidelic coefficient of friction and moments of inertia, Front. Bioeng. Biotechnol. 10 (2022) 860435.
[80] N. Mills, A. Gilchrist, Oblique impact testing of bicycle helmets, Int. J. Impact Eng. 35 (9) (2008) 1075–1086.
[81] N.J. Mills, S. Wilkes, S. Derler, A. Flisch, Fea of oblique impact tests on a motorcycle helmet, Int. J. Impact Eng. 36 (7) (2009) 913–925.
[82] S.J. Bonin, A.L. DeMarco, G.P. Siegmund, The effect of mips, headform condition, and impact orientation on headform kinematics across a range of impact speeds during oblique bicycle helmet impacts, Ann. Biomed. Eng. 50 (7) (2022) 860–870.
[83] N.E.-P. Stark, M. Begonia, L. Viano, S. Rowson, The influence of headform friction and inertial properties on oblique impact helmet testing, Ann. Biomed. Eng. 52 (10) (2024) 2803–2811.
[84] En 12697-31:2019 - bituminous mixtures - test methods - part 31: Specimen preparation by gyratory compactor, 2019. (Accessed 5 March 2025).
[85] O. Sirin, D.K. Paul, E. Kassem, State of the art study on aging of asphalt mixtures and use of antioxidant additives, Adv. Civ. Eng. 2018 (1) (2018) 3428961.
[86] F. Yin, E. Arámbula-Mercado, A. Epps Martin, D. Newcomb, N. Tran, Long-term ageing of asphalt mixtures, Road Mater., Pavement Des. 18 (sup1) (2017) 2–27.
[87] J. Kirchherr, D. Reike, M. Hekkert, Conceptualizing the circular economy: an analysis of 114 definitions, Resour. Conserv. Recycl. 127 (2017) 221–232.
[88] J. Adams, M. Hillman, The risk compensation theory and bicycle helmets, Inj. Prev. 7 (2) (2001) 89–91.
[89] D.L. Robinson, Do enforced bicycle helmet laws improve public health, Br. Med. J. 332 (7543) (2006) 722.
[90] A. Charef, Z. Jarir, Impact of delivery and private riders' roles on safety behavior in Marrakech Morocco, Results Eng. (2025) 105371.

[91] A. Trotta, A.N. Annaidh, R.O. Burek, B. Pelgrims, J. Ivens, Evaluation of the head-helmet sliding properties in an impact test, J. Biomech. 75 (2018) 28–34.

[92] Ó. Juste-Lorente, M. Maza, M. Piccand, F.J. López-Valdés, The influence of head-form/helmet friction on head impact biomechanics in oblique impacts at different tangential velocities, Appl. Sci. 11 (23) (2021) 11318.

[93] A.K. Knutsen, A.D. Gomez, M. Gangolli, W.-T. Wang, D. Chan, Y.-C. Lu, E. Christoforou, J.L. Prince, P.V. Bayly, J.A. Butman, et al., In vivo estimates of axonal stretch and 3d brain deformation during mild head impact, Brain Multiphys. 1 (2020) 100015.

[94] P.V. Bayly, A. Alshareef, A.K. Knutsen, K. Upadhyay, R.J. Okamoto, A. Carass, J.A. Butman, D.L. Pham, J.L. Prince, K. Ramesh, et al., Mr imaging of human brain mechanics in vivo: new measurements to facilitate the development of computational models of brain injury, Ann. Biomed. Eng. 49 (10) (2021) 2677–2692.